PROCEEDINGS OF SCIENCE

Parton Distributions from Lattice and Impacts on Global QCD Analysis

Huey-Wen Lin*

Department of Physics and Astronomy, Michigan State University, East Lansing, MI 48824

E-mail: hwlin@pa.msu.edu

There have been rapid developments in the direct calculation in lattice QCD (LQCD) of the Bjorken-x dependence of hadron structure through large-momentum effective theory (LaMET) and other similar effective approaches. These methods overcome the previous limitation of LQCD to moments (that is, integrals over Bjorken-x) of hadron structure, allowing LQCD to directly provide the kinematic Bjorken-x regions where the experimental values are least known. In this proceeding, I will show some selected recent progress along these directions and examples of how including lattice-QCD calculations in the global QCD analysis can play a significant role in improving our understanding of parton distributions in the future.

The XVIth Quark Confinement and the Hadron Spectrum Conference (QCHSC24)
19-24 August, 2024
Cairns Convention Centre, Cairns, Queensland, Australia

*Speaker

 ISSN 1824-8039 . Published by SISSA Medialab.

PoS(QCHSC24)023

1. Introduction and Background

Parton distribution functions (PDFs) serve as universal descriptors of the quark and gluon content within nucleons, providing a fundamental understanding of their internal structure in terms of momentum distributions. This universality is a cornerstone of high-energy physics, making PDFs essential for interpreting a vast array of experimental data. Consequently, there is significant and growing interest in precisely determining these distributions, evidenced by the many ongoing and planned experiments across the globe at facilities such as BNL, JLab, J-PARC, COMPASS, GSI, and the future Electron-Ion Collider (EIC) and its Chinese counterpart (EicC), as well as the proposed Large Hadron-Electron Collider (LHeC). These experimental efforts are directly motivated by fundamental questions, as articulated by researchers at Confinement 2024, aiming to unravel how the sea quarks and gluons, including their spin contributions, are distributed in both space and momentum inside the nucleon. This quest to "image the proton", as highlighted in the earlier EIC White Paper [1], "The Present and Future of QCD" community whitepaper [2] for the 2023 Nuclear Physics Long Range plan. The synergy between these experimental endeavors and theoretical advancements in calculating PDFs is crucial for achieving a comprehensive picture of nucleon structure.

The determination of PDFs relies on a comprehensive approach known as global analysis. This method capitalizes on the wealth of data obtained from various high-energy physics experiments, which collectively probe a diverse range of kinematic variables relevant to the partonic structure of hadrons. The core of a global analysis involves a simultaneous fit to a multitude of experimental datasets, effectively combining theoretical predictions with experimental measurements. However, it is important to recognize that the resulting PDFs are not solely determined by the data. Several choices made during the analysis procedure significantly influence the outcome. These include the selection of specific experimental datasets and the imposition of kinematic cuts to ensure data quality and relevance. Furthermore, the value adopted for the strong coupling constant at the Z-boson mass, $\alpha_s(M_Z)$, a fundamental parameter in QCD, plays a crucial role in the theoretical calculations. A degree of model dependence is also introduced by the functional form chosen to parametrize the parton distributions at an initial energy scale μ_0, often expressed through a fitting function such as $xf(x,\mu_0) = a_0 x^{a_1}(1-x)^{a_2}P(x)$, where x represents the Bjorken scaling variable and $P(x)$ can be in polynomial functions in x. Finally, global analyses typically incorporate certain theoretical assumptions to constrain the fit, such as $SU(3)$ flavor symmetry, charge symmetry relations between quark distributions (e.g., $u_v^p(x) = d_v^n(x)$), and specific models for the strange ($s(x), \bar{s}(x)$) and sea ($\bar{u}(x), \bar{d}(x)$) quark distributions, often expressed in relations like $s(x) = \bar{s}(x) = \kappa(\bar{u}(x) + \bar{d}(x))$, where κ is a constant factor. Consequently, the derived PDFs represent a synthesis of experimental constraints and theoretical frameworks, shaped by the specific choices and assumptions inherent in the global-analysis procedure. Global-analysis PDFs from different choices of parameters, assumptions and experimental inputs are consistent with each other in the x region where there is plenty of data to constrain the fits. In the region where there is less data, such as for the strange, or for large x in the gluon and d-quark distributions, the resulting PDF can have very different extrapolations into these less determined regions. While waiting for future experimental data from the LHC or EIC, we can make progress by providing complementary constraints using reliable nonperturbative QCD theoretical calculations.

Lattice quantum chromodynamics (LQCD) is an ideal theoretical tool for investigating the strong-coupling regime of quantum field theories. In LQCD, physical observables, denoted by $\langle O(\bar{\psi}, \psi, A)\rangle$, are calculated from the path integral formulated in Euclidean space:

$$\langle O(\bar{\psi}, \psi, A)\rangle = \frac{1}{Z}\int DA\, D\bar{\psi}\, D\psi\, e^{iS(\bar{\psi},\psi,A)} O(\bar{\psi}, \psi, A),$$

where A represents the gluon field, ψ and $\bar{\psi}$ the quark and antiquark fields, and S the action. LQCD imposes an ultraviolet (UV) cutoff by discretizing spacetime onto a lattice with spacing a. Like continuum QCD, LQCD also needs a quark-mass parameter, often related to the pion mass m_π; since calculations involving heavier quark mass make it easier to accumulate the necessary signal-to-noise ratio in results, it is common practice to test out new methods using heavier-than-nature up/down-quark mass before performing the expensive calculations with realistic quark masses. To make these calculations tractable, LQCD imposes an infrared (IR) cutoff by considering a finite volume $L^3 \times T$. Ultimately, to recover the physical limit, we need to extrapolate the LQCD results to the physical pion mass m_π^{phys} if not directly calculating at m_π^{phys}, zero lattice spacing ($a \to 0$), and infinite volume ($L \to \infty$).

Traditional LQCD calculations for PDFs have primarily relied on the operator product expansion (OPE), which inherently only provides information about the moments of these distributions. For spin-averaged or unpolarized PDFs, $q(x)$, the nth moment is given by $\langle x^{n-1}\rangle_q = \int_{-1}^{1} dx\, x^{n-1} q(x)$. Similarly, for spin-dependent longitudinally polarized PDFs, $\Delta q(x)$, the n-th moment is $\langle x^{n-1}\rangle_{\Delta q} = \int_{-1}^{1} dx\, x^{n-1}\Delta q(x)$. Finally, for spin-dependent transversely polarized PDFs, $\delta q(x)$, the n-th moment is $\langle x^{n-1}\rangle_{\delta q} = \int_{-1}^{1} dx\, x^{n-1}\delta q(x)$. The spin-averaged/unpolarized moments are the most well known and best determined, while the spin-dependent transversely polarized moments are very poorly known. A crucial limitation of this approach is that the true x-dependence of the distribution can only be fully recovered if all moments are known, which is practically impossible to achieve in lattice calculations.

Figure 1 highlights the synergistic relationship between LQCD calculations and the global analysis of transversity PDFs. Lattice calculations offer a nonperturbative approach to understanding the quark and gluon structure of hadrons from first principles, providing complementary information to experimental measurements. The inclusion of lattice results in global fits helps to constrain PDFs in kinematic regions where experimental data may be limited or less precise. The example plots in the middle and right-hand side of the figure illustrate this synergy by presenting lattice-derived results for the up (h_1^u) and down (h_1^d) quark transversity distributions within the nucleon. The lattice provides well determined physical-continuum–limit tensor charges, which constrain the integral over the region between h_1^u and h_1^d, but this tells us nothing about the shape of the x-dependent transversity PDFs. This must be determined by the experimental data, which when combined with lattice constraints allows us to gain much improved knowledge of the PDF. Furthermore, the favored $zH_{1\,(\text{fav})}^{\perp(1)}$ and unfavored $zH_{1\,(\text{unf})}^{\perp(1)}$ Collins fragmentation functions (FFs) that lattice cannot calculate are also much improved. Together, we unveil much more about nucleon structure than with experimental or lattice inputs alone.

Due to rotational symmetry breaking, lattice calculations are practically limited to the lowest few moments. This is because for higher moments, the operators involved in the calculation tend to mix with lower-dimension operators, introducing significant complications in the renormalization

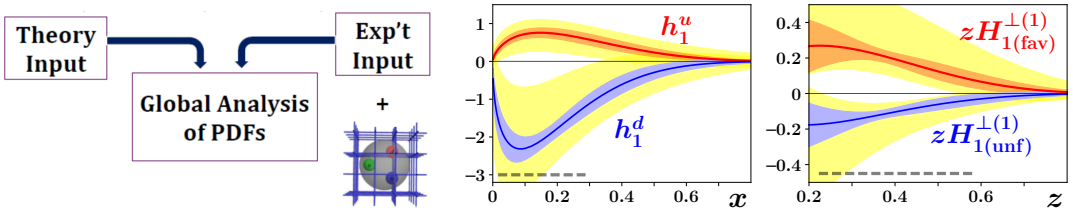

Figure 1: (left) The global QCD analysis can take in not only experimental data but also lattice inputs to better constrain the PDFs, GPDs, or other structure, especially in kinematic regions where experimental data is not as precise and/or difficult to obtain. Example of impacts with LQCD input on the global QCD analysis. Transversity PDFs $h_1^{u,d}$ (middle) and favored $zH_{1\,(\text{fav})}^{\perp(1)}$ and unfavored $zH_{1\,(\text{unf})}^{\perp(1)}$ Collins FFs (right) for the SIDIS+Lattice-QCD g_T constraint (red and blue bands) at $Q^2 = 2$ GeV^2, compared with the SIDIS-only fit uncertainties (yellow bands). The range of direct experimental constraints is indicated by the horizontal dashed lines. Figures taken from Ref. [3].

procedure and increasing uncertainties and/or making the continuum limit impossible. To overcome this inherent problem, there have been several novel theoretical proposals and computational techniques have been developed; see reviews in Refs. [4–6]. The challenge of directly accessing the x-dependence of hadron structure quantities has been a longstanding obstacle in the field, and was often considered the "holy grail" of structure calculations. This limitation is not unique to PDFs but applies to a wide range of crucial structure quantities, hindering our ability to obtain a complete multidimensional picture of nucleon structure. Overcoming this obstacle is therefore a central focus of ongoing theoretical developments and computational efforts in the lattice-QCD community.

A significant advancement in addressing the limitations of traditional lattice calculations for PDFs is the development of the Large-momentum effective theory (LaMET), also known as the quasi-PDF approach, pioneered by X. Ji [7] and reviewed in subsequent work [4]. This method proposes to compute a quasi-distribution, denoted by $\tilde{q}(x,\mu,P_z)$, directly on the lattice through the following formula:

$$\tilde{q}(x,\mu,P_z) = \int_{-\infty}^{\infty} \frac{dz}{4\pi} e^{-izk_z} \langle P|\bar{\psi}(z)\Gamma \exp\left(-ig\int_0^z dz' A_z(z')\right)\psi(0)|P\rangle,$$

where $|P\rangle$ represents a nucleon state with large momentum P_z in the z-direction, ψ and $\bar{\psi}$ are the quark fields, Γ is an appropriate Dirac matrix, and the exponential term is a Wilson line ensuring gauge invariance. The true physical lightcone distribution $q(x,\mu)$ is then recovered by taking the $P_z \to \infty$ limit. The relationship between the quasi-distribution and the true distribution involves a matching procedure can be expressed as

$$\tilde{q}(x,\mu,P_z) = \int_{-1}^{1} \frac{dy}{|y|} C\left(\frac{x}{y}, \frac{\mu}{yP_z}\right) q(y,\mu) + O\left(\frac{M_N^2}{P_z^2}, \frac{\Lambda_{\text{QCD}}^2}{x^2P_z^2}, \frac{\Lambda_{\text{QCD}}^2}{(1-x)^2P_z^2}\right),$$

where C is a Wilson coefficient, M_N is the nucleon mass, and Λ_{QCD} is the QCD scale. LaMET introduces a new source of systematic uncertainties related to the finite momentum P_z of the nucleon state used in the lattice calculations. While smaller values of P_z often lead to better statistical signals in the lattice computations, they simultaneously result in larger systematic errors in the matching

procedure used to extract the physical PDFs. This inverse relationship between statistical precision and systematic control with respect to P_z is analogous to the situation encountered with the pion mass in traditional lattice calculations, where heavier pion masses can yield better precision but necessitate larger extrapolations to the physical pion mass. Consequently, the momentum P_z becomes a crucial new parameter in these x-dependent methods that requires careful attention and systematic study to ensure the reliability and accuracy of the extracted parton distributions.

There are rapid developments in other x-dependent methods as well, aiming to directly access parton distributions and related quantities from lattice QCD calculations. These approaches generally involve computing quantities that are calculable on the lattice today and relating them to the wanted PDFs, GPDs, etc., through a convolution with a perturbatively calculated kernel, often within a similar framework like quasi-PDF/LaMET. Besides LaMET, other prominent methods include the Pseudo-PDF method, which differs in its Fourier transform approach; the Lattice Cross-Section (LCS) method; methods based on Compton amplitudes; calculations of hadronic tensor currents; and the use of Euclidean correlation functions (see reviews and references in Refs. [4–6].). These diverse approaches signify a vibrant and evolving field dedicated to overcoming the traditional limitations of lattice calculations and providing direct access to the x-dependence of hadron structure.

Figures 4 and 5 in Ref. [6] present a chronological overview of first numerical results due to a proposed x-dependent method and first achievements in lattice parton calculations over the past decade (2013–2023). Starting with the first unpolarized lattice PDF in 2013, the field has witnessed substantial progress, including the crucial step of reaching physical quark masses in PDF calculations around 2016. The timeline further showcases the computation of pion valence PDFs, polarized PDFs with mass corrections, pion and kaon distribution amplitudes, and the extension to more complex quantities like GPDs, with the first pion GPD calculation around 2020. The latter part of the timeline emphasizes the increasing sophistication of lattice calculations, enabling the determination of kaon PDFs and gluon PDFs for both the nucleon and the pion, demonstrating the continuous advancements in our understanding of hadron structure from the first principles of QCD.

2. Selected x-Dependent Parton Distributions

Since 2013, there has been much progress in nucleon isovector lattice-QCD PDF calculations; the field has moved on to calculations either directly at or extrapolating to the physical pion mass with these quantities. Among all the leading twist-2 PDF calculations, the nucleon isovector unpolarized PDFs has been most calculated. Global fitting uses more than a half century of experimental data to reconstruct the proton unpolarized PDFs. As a result, we can use the unpolarized channel as a benchmark to understand better the lattice systematics, and in return, we can use these systematics to apply lattice polarized PDF predictions, such as helicity and transversity. The lattice setup and procedure for these three twist-two PDFs are exactly the same but up to a different γ matrix. These lattice-calculated polarized PDFs can be used to extend our knowledge in these less experimentally known PDFs and other structure functions.

Figure 2 shows a summary of lattice-QCD calculations of the nucleon isovector unpolarized (left), helicity (middle) and transversity (right) PDFs either directly at the physical pion mass (LP3 and ETMC) or extrapolated to physical pion mass (JLab/W&M); plots and references can be found

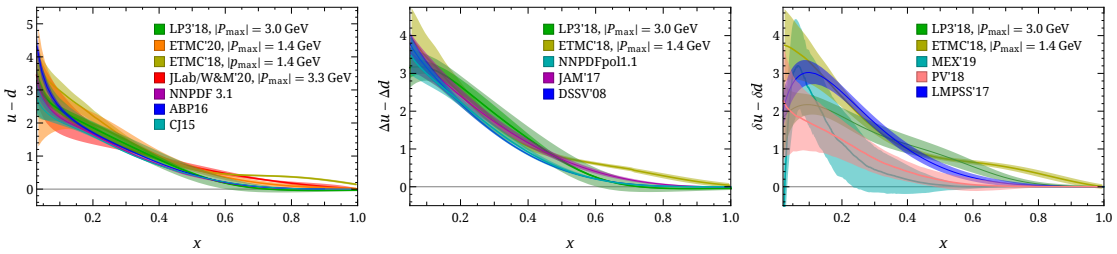

Figure 2: Summary of lattice calculations of isovector unpolarized (left), helicity (middle) and transversity (right) with LP3 and ETMC isovector quark taken from LP318, ETMC20/ETMC18, JLab/W&M valence unpolarized distribution results, and global fits from NNPDF3.1, CJ15, NNPDFpol1.1, JAM17, DSSV08, MEX19, PV18, LMPSS17, taken from Ref. [5]. Note that none of the current lattice calculations have taken the continuum limit ($a \to 0$) and have remaining lattice artifacts (such as finite-volume effects); disagreement in the obtained distributions is not unexpected.

in Ref. [5]. Note that none of the lattice calculations shown are performed in the continuum limit yet (that is, they are only done at one lattice spacing, lack finite-volume extrapolation, etc., in addition to using different nucleon boost momenta and systematics treatments); therefore, one should not expect them to be consistent with each other yet. However, one can see that the lattice results provides roughly the similar magnitude results. The lattice-calculated unpolarized PDFs, especially those performed with larger boost momentum, are in good agreement with the selected global fits shown in the figure. However, the current lattice results have much larger errors than those obtained from global fits. This should not be too surprising, since these new x-dependent calculations are barely one decade old, competing with eighty years of experimental data in the global fits. With more computational resources, lattice PDF errors can be further reduced. On the other hand, the lattice helicity PDFs have more competitive statistical errors with the global fits. However, since the experimental data are more limited in the polarized cases due to the difficulty in creating high polarization in target or beam, more assumptions have to be made in the helicity global-fit PDF. The statistical accuracy of the lattice transversity PDF results is even better than current phenomenological determinations, due to the difficulty in experimental data collection as well as complications in the theoretical inputs into the global-QCD analysis. With more computational resources, lattice calculations can overcome the current limitations of the lattice systematics and use larger boost momentum to extend the x region expected to be reliable.

There have been several recent updates to the lattice calculations. In systematics, there have been LQCD calculations of the unpolarized nucleon isovector PDFs at the physical pion mass [8] with a sophisticated theoretical framework employed, including next-to-next-to-leading order (NNLO) matching and careful treatment of leading-renormalon effects through techniques like Leading-Renormalon Resummation (LRR) and Renormalization-Group Resummation (RGR) [9]. The comparison between different perturbative treatments (NNLO, NNLO×RGR, NNLO+LRR, (NNLO+LRR)×RGR) highlights the theoretical uncertainties and the impact of resummation techniques on the extracted PDFs. ANL/BNL group has also reported an updated isovector transversity distribution at physical pion mass with lattice spacing 0.076 fm with NLO and LRR+RGR improvement [10]. There has been also progress made in the continuum-limit nucleon PDFs. The MSULat collaboration employed clover/2+1+1 HISQ fermions with several lattice spacings and pion

masses to facilitate the extrapolation to the physical continuum for unpolarized nucleon isovector PDFs [11]. LPC collaboration also made progress in a continuum-limit transversity PDF using clover/2+1 clover fermions at multiple lattice spacings and pion masses, and compared against phenomenological extractions [12]. One would expect future lattice PDF calculations to be done in the continuum limit and more theoretical systematic improvements to increase the precision of the LQCD PDFs.

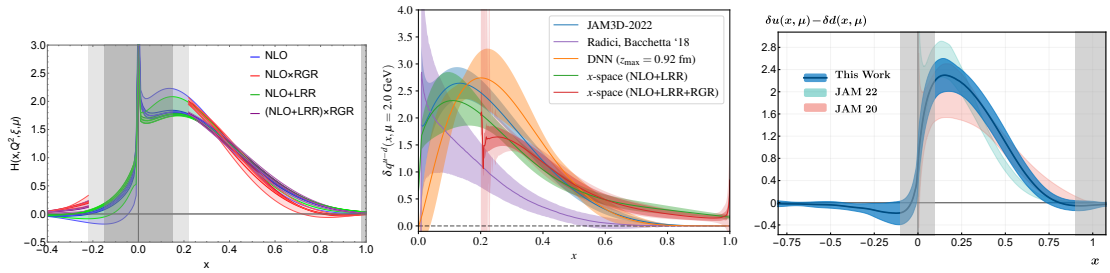

Figure 3: (left) Unpolarized isovector nucleon lightcone PDFs at NLO and NNLO with/without LRR and RGR improvements by MSULat [8]. (middle) The isovector nucleon transversity PDFs at NLO+LRR and NLO+LRR+RGR using the LaMET framework with the largest momentum $P_z \approx 1.5$ GeV with comparisons with the extraction using DNN method and with the global analysis from JAM3D-22; plot taken from Ref. [10]. (right) Isovector nucleon transversity PDF normalized to the nucleon isovector tensor charge g_T by LPC collaboration with lattice results extrapolated to the continuum, physical pion mass and those from JAM20 JAM22 global fits; plot taken from Ref. [12].

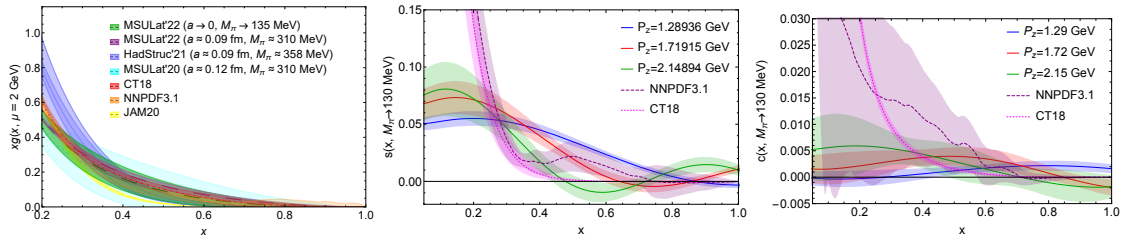

Figure 4: (right) The $N_f = 2 + 1 + 1$unpolarized gluon PDF $xg(x, \mu)$ obtained from the NLO fit to the lattice data at pion masses $M_\pi = 135$ (extrapolated) [13], compared with the NNLO CT18 and NNPDF3.1 gluon PDFs. The $x > 0.3$ PDF results are consistent with the NNLO CT18 and NNPDF3.1 unpolarized gluon PDFs in $\overline{\text{MS}}$ scheme at $\mu = 2$ GeV [13]. The x-dependent strange (middle) and charm (right) PDF from a naive truncated inverse Fourier transformation and inverse matching for $P_z = \{1.29, 1.72, 2.15\}$ GeV extrapolated to physical pion mass [14].

There has been some progress made in the flavor-singlet PDFs but further systematics must be addressed to reach the precision of the flavor nonsinglet results. The left-hand side of Fig. 4 shows a state-of-the-art LQCD determination of the gluon PDF in the nucleon $xg(x)$ employing the pseudo-PDF method and extrapolated to the continuum limit from MSULat work, along with other calculations and global-fit results for comparison [13]. The green bands represent the continuum-physical limit gluon PDF obtained by MSULat, while the purple bands show results from the single-ensemble analysis at 0.09-fm lattice spacing and 310-MeV pion mass. Both results are consistent with global-fit PDFs from CT18 and NNPDF3.1 NNLO analyses for x values in the range $[0.25, 1]$,

though deviations are observed for $x < 0.3$. The continuum-physical–limit results have larger uncertainties due to the extrapolation process, while the single-ensemble results exhibit smaller errors, comparable to those of CT18 and NNPDF3.1. There is a potential tension with the JAM20 global-fit gluon PDF for $x < 0.6$, which behaves slightly differently from CT18 and NNPDF3.1. Additionally, the figure compares the current results with prior lattice-QCD calculations, including those from MSULat and HadStruc collaborations. The cyan bands represent MSULat's earlier pseudo-PDF calculation, while the blue bands show HadStruc's results using a different lattice setup and methodology. The current single-ensemble results (purple bands) show noticeable deviations from HadStruc's results, particularly in the large-x region, where HadStruc's gluon PDF is significantly smaller. However, methodological differences, such as the choice of gluon operators and renormalization strategies, make direct comparisons challenging. Despite these differences, the continuum-physical limit results (green bands) are consistent with prior single-ensemble lattice calculations due to larger total uncertainties from the extrapolation process. Future work incorporating finer lattice spacings and lighter pion masses is expected to improve the precision of the continuum-physical gluon PDF.

The first lattice-QCD calculation of the unpolarized strange and charm PDFs using LaMET was done by MSULat with 0.12-fm lattice spacing and extrapolated to physical pion mass [14]. The middle and right-hand side of Fig. 4 shows naive extraction of the x-dependent strange and charm PDFs using truncated inverse Fourier transformations and inverse matching for boost momenta $P_z = \{1.29, 1.72, 2.15\}$ GeV at the extrapolated physical pion mass. The results show significant suppression in the smaller-x region due to the lack of contributions from larger-z values, which are expected to be substantial but beyond the computational capability of lattice calculations. Additionally, the momentum dependence is evident, as different boost momenta correspond to varying truncation ranges of zP_z. This highlights the limitations of the current approach and the need for larger-z contributions to reliably capture the x-dependence of the PDFs. A comparison with the CT18NNLO and NNPDF3.1NNLO global fits is also shown.

Generalized parton distributions (GPDs) are crucial for a comprehensive understanding of nucleon structure, going beyond simpler descriptions by unifying spatial and momentum distributions of quarks and gluons. They enable a 3D tomographic view of the nucleon and provide access to the orbital angular momentum of partons, vital for solving the nucleon spin puzzle. GPDs are the theoretical foundation for interpreting hard exclusive scattering experiments and are connected to fundamental nucleon properties like form factors and mass distribution. The experimental efforts at facilities like Jefferson Lab and the future Electron-Ion Collider (EIC) heavily rely on the theoretical framework of GPDs. The unpolarized GPDs $H(x, \xi, t, \bar{P}_z)$ and $E(x, \xi, t, \bar{P}_z)$ can be related to the via nucleon matrix elements

$$\frac{\bar{P}_z}{P_0} \int \frac{dz}{4\pi} e^{ixzP_z} \langle P'|\bar{\psi}\gamma_0(z)\psi(0)|P\rangle = \frac{\bar{u}(P')}{2\bar{P}^0} \left(H(x, \xi, t, \bar{P}_z)\gamma^0 + E(x, \xi, t, \bar{P}_z) \frac{i\sigma^{0\mu}\Delta_\mu}{2M} \right) u(P'')$$

where the kinematic variables are $p^\mu = \frac{p''^\mu + p'^\mu}{2}$, $\Delta^\mu = p''^\mu - p'^\mu$, $t = \Delta^2$, and $\xi = \frac{p''^+ - p'^+}{p''^+ + p'^+}$. Figure 5 shows two different ways performing a lattice calculation of the GPD: the traditional Breit (symmetric) frame and the "asymmetric" frame that connects $H\left(z \cdot P^{s/a}, z \cdot (\Delta^{s/a})^2\right) =$

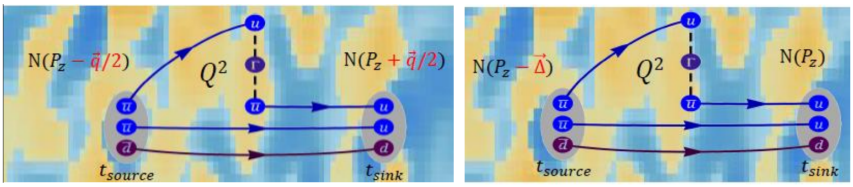

Figure 5: Breit (symmetric, left) and asymmetric-frame lattice setup for GPD calculations

$A_1 + \frac{\Delta^{s/a}\cdot z}{P^{s/a}\cdot z} A_3$ with amplitudes defined by

$$F^\mu(z,P,\Delta) = \bar{u}(p_f,\lambda')\left[\gamma^\mu A_1 + \frac{P^\mu}{m}A_2 + \frac{\Delta^\mu}{m}A_3 + im\sigma^{\mu\nu}\frac{\Delta_\nu}{m^2}A_4 + \frac{i\sigma^{\mu\Delta}}{m}A_5 + \frac{P^\mu i\sigma^{z\Delta}}{m^2}A_6 + \frac{\Delta^\mu i\sigma^{z\Delta}}{m^2}A_7 + \frac{\Delta^\mu i\sigma^{i\Delta}}{m^2}A_8\right]u(p_i,\lambda).$$

[15, 16]

Figure 6 shows state-of-the-art lattice calculations in both frames. The left-hand side and middle of Fig. 6 show MSULat's 3D visualizations of the isovector nucleon GPDs, specifically $H(x,\xi=0,Q^2)$ and $E(x,\xi=0,Q^2)$, obtained in Breit frame at the physical pion mass [17]. The MSULat collaboration utilized a clover/2+1+1 HISQ fermion action with a lattice spacing of roughly 0.09 fm and a pion mass of 135 MeV, with a nucleon momentum of about 2 GeV and fixed skewness parameter $\xi = 0$. Since this was the first lattice x-dependent GPD with multiple transfer momenta Q^2, MSUlat tested their result by taking the x-integral for the second Mellin moment $(n=2)\int_{-1}^{+1} dx\, x^{n-1}\{H,E\}(x,\xi=0,Q^2) = \sum_{i=0,\text{even}}^{n-1}\left((-2\xi)^i\{A,B\}^q_{ni}(t) - (-2\xi)^n C^q_{n0}(t)\right)\Big|_{n\ \text{even}}$ and comparing to existing calculations at physical pion mass of the isovector electric and magnetic form factors $G_{\{E,M\}}(Q^2)$ and generalized form factors $\{A,B\}_{20}(Q^2)$ using the traditional moment operator; these were found to be in reasonable agreement. Building upon the LQCD calculations of nucleon GPDs, MSULat also presented a glimpse into nucleon tomography, revealing the spatial distribution of quarks within the nucleon for the first time. A similar study of the polarized GPD can be found in Ref. [18]. The right-hand side of Fig. 6 presents an example of the isovector nucleon GPD calculated in asymmetric frame by the ANL/BNL/ETMC collaboration at 260-MeV pion mass, momentum boost 1.3 GeV and zero skewness with $Q^2 \in [0.17, 2.24]$ GeV^2. Note that the asymmetric frame allows one to incorporate more momentum transfers without increasing the computational cost at an given P_z; thus, more transfer momenta can be researched than in the Breit frame.

There have been efforts to improve the systematics of the flavor-singlet PDFs and GPDs. The systematic improvements emphasize the sophisticated theoretical framework employed, which incorporates NNLO matching and the treatment of leading-renormalon effects through both Leading-Renormalon Resummation (LRR) and Renormalization-Group Resummation (RGR) [9]. The right-hand side of Fig. 7 presents the first systematic investigation into the calculation of nucleon isovector GPDs using lattice QCD at the physical pion mass. The zero-skewness GPD $H(x,\xi=0,\mu^2)$ as a function of the longitudinal momentum fraction x, evaluated at a fixed momentum transfer $Q^2 = 0.39$ GeV^2 at different levels of NLO and NNLO perturbative accuracy and resummation improvement. The result highlights the importance of these theoretical improvements for obtaining

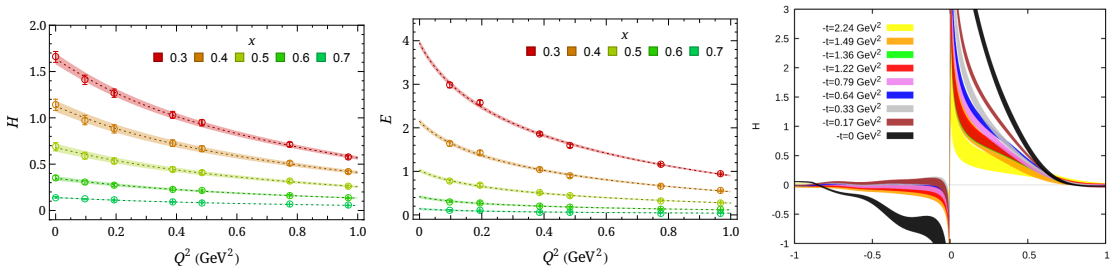

Figure 6: Nucleon isovector H (left) and E (middle) GPDs at $\xi = 0$ with z-expansion to Q^2 at selected x values, calculated in Breit frame at physical pion mass. (right) H quasi-GPD plot taken from Ref. [19] calculated at 260-MeV lattice with the nucleon boost momentum at 1.25 GeV in asymmetric frame

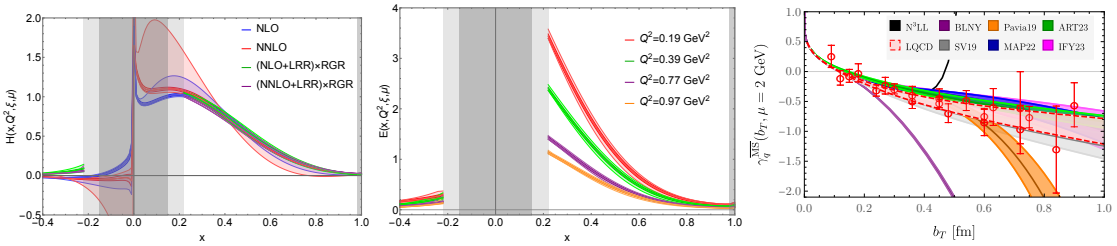

Figure 7: (left) Example of lightcone H GPDs with NLO (blue), NNLO (red), and their application with resummation (green and purple) evaluated at $Q^2 = 0.39$ GeV^2 and $\xi = 0$; plot taken from Ref. [8]. The inner bands are statistical errors while the outer bands are combined statistical and systematic errors, derived from the scale variation, the dark-gray regions are the x-values at which the LaMET calculation breaks down. In addition, when RGR is applied, the matching formula breaks down for $|x| \lesssim 0.2$, which is shaded in light gray. (NNLO + LRR) $\times$ RGR E GPDs at $\xi = 0$ and variable Q^2 with inner/outer error bands are statistical and combined statistical and systematic errors respectively; plot taken from Ref. [8] (right) Comparison of lattice QCD parameterization of the CS kernel compared with phenomenological parameterizations of experimental data (BLNY, SV19, Pavia19, MAP22, ART23, IFY23), and N^3LL perturbative results; plot taken from Ref. [20].

precise and reliable GPDs from lattice calculations [8]. The middle of Fig. 7 shows the dependence on transfer-momentum squared $Q^2 \in [0.19, 0.97]$ GeV^2 of GPD $E(x, Q^2, \xi, \mu)$ after incorporating the highest level of theoretical corrections discussed previously, namely the (NNLO+LRR)×RGR treatment. The different curves clearly show how the shape and magnitude of the GPD E change as the resolution scale Q^2 increases, reflecting the QCD evolution of the parton distributions within the nucleon. This Q^2 dependence is crucial for connecting lattice calculations to experimental measurements performed at various energy scales and provides a more complete understanding of the nucleon's complex internal structure.

Transverse-momentum–dependent distributions (TMDs) are essential for understanding the confined motion of partons inside hadrons. A generic TMD $f(x, k_T, \mu, \eta)$ includes variables describing the longitudinal momentum fraction x and the transverse momentum k_T of a quark within a polarized nucleon, as well as the energy scale μ and a regularization parameter η. TMDs can link between the one-dimensional momentum distributions of PDFs and provide information for the more complex, multidimensional Wigner distributions, and then GPDs. By incorporating the transverse momentum of partons, TMDs offer to complete a richer and more nuanced description

of the nucleon's 3D structure. To access these structure on the lattice, one can attempt to relate quasi-TMDs ($\tilde{f}^{\rm TMD}$) on the lattice to lightcone TMDs ($f^{\rm TMD}$) [21]

$$\tilde{f}^{\rm TMD}(x,\vec{b}_T,\mu,P^z) = C^{\rm TMD}(\mu,xP^z)g_S(b_T,\mu)\exp\left[-\frac{1}{2}K(b_T,\mu)\log\left(\frac{(2xP^z)^2}{\mu^2}\right)\right]\times f^{\rm TMD}(x,\vec{b}_T,\mu,\zeta)+O\left(\frac{q_T^2\Lambda_{\rm QCD}^2}{P_z^2}\right)+\Theta\left(\frac{q_T^2}{P_z^2}\right)$$

where $K(b_T,\mu)$ is Collins-Soper kernel and $g_S(b_T,\mu) \sim \sqrt{S_T(b_T,\mu)}$ is the soft function. The TMD is obtained from the quasi-TMD through a convolution involving a perturbative matching coefficient $C^{\rm TMD}$, with known $K(b_T,\mu)$ and $g_S(b_T,\mu)$. Lattice QCD can improve TMD knowledge by providing nonperturbative constraints on key quantities like the CS kernel, which governs the rapidity evolution of TMDs. This is particularly valuable in regions where phenomenological extractions from experimental data are largely unconstrained, such as at small transverse momentum scales ($q_T < 0.3$ GeV). The right-hand side of Fig. 7 a state-of-the-art CS kernel calculation from lattice QCD combined with LaMET, compared various phenomenological parameterizations derived from experimental data (BLNY, SV19, Pavia19, MAP22, ART23, and IFY23), as well as perturbative results at N^3LL accuracy. The LQCD results align closely with recent phenomenological parameterizations which incorporate modern global fits of experimental data; in contrast, older parameterizations like BLNY show significant deviations, particularly at large transverse displacement b_T. This consistency with recent models highlights the precision of the lattice QCD approach and its ability to disfavor outdated parameterizations, reinforcing its value in constraining the CS kernel in nonperturbative regions [20]. More examples of the lattice TMD efforts can be found in these review articles [4, 5].

3. Impact of Lattice-QCD PDFs on Global Fits

A 2020 LQCD study investigated the strangeness asymmetry within the nucleon $s(x) - \bar{s}(x)$, computed on a single 0.12-fm lattice ensemble, renormalized nonperturbatively and extrapolated to the physical pion mass [14]. The lattice results for the real coordinate-space quasi-PDF matrix elements indicate a strangeness asymmetry that is largely consistent with zero within the 95% confidence level: $\mathrm{Re}[h(z)] \propto \int dx\,(s(x) - \bar{s}(x))\cos(xzP_z)$. With a nucleon boost momentum of approximately 1.7 GeV, the renormalized matrix elements are Fourier transformed into quasi-PDFs, followed by the matching procedure from the quasi-PDF ($\tilde{f}_q(x,P_z)$) to the lightcone PDF ($f_q(x,Q)$). The resulting LQCD strangeness asymmetry $x(s(x,Q) - \bar{s}(x,Q))$ is shown on the left-hand side of Fig. 8 over the range 0.3 to 0.8, along with the global fit CT18As at energy scale $Q = 1.3$ GeV. The experimental challenge in measuring the strangeness asymmetry $s(x,Q) - \bar{s}(x,Q)$ at larger values of x ($x > 0.2$) highlights the capability of lattice QCD to provide theoretical predictions for this important aspect of nucleon structure.

The left-hand side of Fig. 8 shows the strange quark PDF $s(x,Q)$ and the strangeness asymmetry $s(x,Q) - \bar{s}(x,Q)$ as functions of x at $Q = 1.3$ GeV, comparing lattice results "$(s - \bar{s})$, Lattice", extrapolated to the physical pion mass, a global fit with and without lattice input, "CT18As NNLO", "CT18As+Lattice", and anticipated improvement with lattice inputs if the current lattice errors are

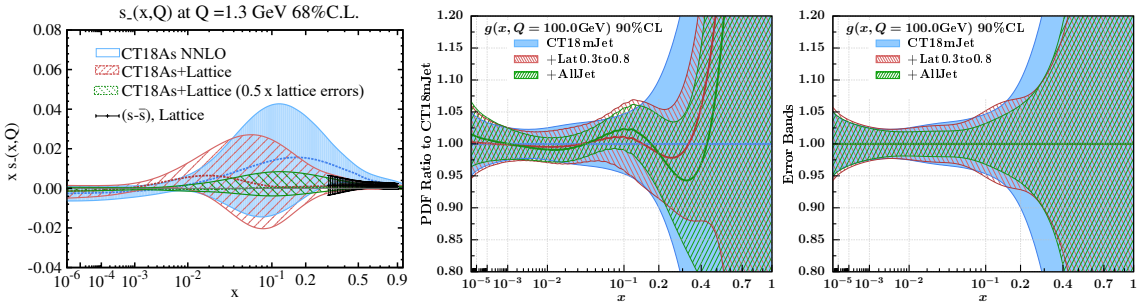

Figure 8: (left) Impact of LQCD calculations (black dashed area) on the difference between strange quark and antiquark PDFs in the recent global fit CT18As NNLO; plot taken from Ref. [22]. The red (green) error bands are obtained with the current (reduced by 50%) LQCD errors. (middle, right) Impact of lattice gluon and CT18 without jet datasets and inclusion of the jet data on the CT18 gluon PDF. Figures taken from Ref. [23].

reduced by another factor of 2, "CT18As+Lattice (0.5 × lattice error)". Together with experimental data and latices inputs, we are able to provide complementary information for the strangeness asymmetry, which is hard to access experimentally at $x > 0.2$, and make an impact in the small-x region to 10^{-6}, where it is currently challenging for lattice QCD to provide reliable calculations.

Reference [23] investigates the impact of recent LQCD gluon parton distribution function results on global PDF analysis within the CTEQ-TEA framework, focusing on large-x regions and their implications for high-energy collider processes. To study the possible lattice impacts on the gluon PDF, consider the state-of-the-art lattice nucleon gluon PDF study by MSULat, which utilized 2 + 1 + 1 HISQ fermions with lattice spacings of approximately 0.09, 0.12, and 0.15 fm, and pion masses of 220, 310, and 700 MeV, with a subsequent extrapolation to both the continuum limit and the physical pion mass [13]. Reference [23] utilized two LQCD gluon-PDF results from MSULat in a global fit: the physical-continuum limit ($a \to 0$, $M_\pi \approx 135$ MeV) and a single ensemble ($M_\pi \approx 310$ MeV, $a \approx 0.09$ fm), allowing a comparison of current and future LQCD gluon PDF uncertainties, respectively. It was shown that there is consistency between these current and future results within their self-consistently determined uncertainties. Given a maximum boost momentum of about 2.6 GeV, lattice PDF inputs are conservatively restricted to $x \in [0.3, 0.8]$ or $[0.4, 0.7]$, where systematic uncertainties are smaller and experimental constraints are weak.

Figure 8 showcases the impact of the first study of the gluon PDF using the pseudo-PDF approach from lattice QCD. The impact of incorporating lattice gluon datasets ("Lat0.3to0.8" and "Lat0.4to0.7") into the CT18 global fit on the gluon PDF at $Q = 100$ GeV was illustrated in Ref. [23]. The inclusion of lattice inputs results in a harder gluon distribution at large x ($x > 0.3$) and a softer distribution at intermediate x ($10^{-2} < x < 10^{-1}$). Additionally, the uncertainty bands for the gluon PDF are significantly reduced in the large-x region, showcasing the constraining power of LQCD data in complementing existing experimental datasets. The middle and left of Fig. 8 compare the impact of lattice gluon datasets ("Lat0.3to0.8") and collider jet datasets ("AllJet") on the gluon PDF using the "CT18mJet" (CT18 standard fit without any jet data) baseline, which excludes all inclusive jet datasets. The analysis shows that the lattice dataset primarily constrains the gluon PDF in the large-x region ($x > 0.3$), while the "AllJet" datasets provide broader constraints across the entire

x range, including intermediate-x ($x < 0.3$). For $x > 0.5$, the lattice dataset exhibits comparable or stronger constraining power than the AllJet datasets, highlighting its unique role in addressing large-x uncertainties where experimental data is sparse or less precise. This demonstrates the complementary nature of LQCD inputs and collider jet datasets in refining the gluon PDF. Several phenomenological implications at the LHC, focusing on gluon-gluon parton luminosity and related processes, such as the production of a Higgs-like scalar, top-quark pairs, and their associated production with an additional jet, Higgs, or Z boson, can also be found in Ref. [23].

4. Conclusion and Outlook

We are entering an exciting era in the study of x-dependent parton distributions, where advances in LQCD are overcoming longstanding limitations. The Bjorken-x dependence of PDFs, which has historically been challenging to access directly from the lattice due to limitations in Euclidean spacetime, is now being widely studied using novel theoretical frameworks and computational techniques. This breakthrough is opening new avenues for understanding the fundamental structure of hadrons directly from lattice QCD and promises to provide crucial nonperturbative input for global PDF analyses. While significant progress has been made in calculating these fundamental quantities, further systematic studies in these new methods are in progress to rigorously assess and control potential uncertainties, ensuring the reliability and impact of these lattice determinations. It is important to note that this overview did not cover many other parallel advancements, such as higher-twist GPDs, meson distribution amplitudes, and other related quantities, where there is also significant progress. Lattice calculations of strange and gluon PDFs have the potential for significant impact in areas where experimental constraints are less precise. The prospect of treating carefully validated lattice matrix elements as direct experimental input in future global PDF fitting procedures represents a paradigm shift in how we determine these fundamental quantities. Ultimately, the pursuit of higher precision and expanded scope in this vital field is limited by the availability of computational resources and the efforts of skilled researchers. Community support will be critical for lattice QCD to make the necessary progress to play an important role in advancing our knowledge of parton distributions.

Acknowledgements

HL thanks the MILC Collaboration for sharing the lattices used to perform many of the parton-distribution studies quoted in this review. The work of HL are partially supported by the US National Science Foundation under grant PHY 1653405 “CAREER: Constraining Parton Distribution Functions for New-Physics Searches”, grant PHY 2209424, by the U.S. Department of Energy under contract DE-SC0024582, and by the Research Corporation for Science Advancement through the Cottrell Scholar Award.

References

[1] A. Accardi, et al., Electron Ion Collider: The Next QCD Frontier: Understanding the glue that binds us all, Eur. Phys. J. A 52 (9) (2016) 268. arXiv:1212.1701, doi:10.1140/epja/i2016-16268-9.

[2] P. Achenbach, et al., The present and future of QCD, Nucl. Phys. A 1047 (2024) 122874. arXiv:2303.02579, doi:10.1016/j.nuclphysa.2024.122874.

[3] H.-W. Lin, W. Melnitchouk, A. Prokudin, N. Sato, H. Shows, First Monte Carlo Global Analysis of Nucleon Transversity with Lattice QCD Constraints, Phys. Rev. Lett. 120 (15) (2018) 152502. arXiv:1710.09858, doi:10.1103/PhysRevLett.120.152502.

[4] X. Ji, Y.-S. Liu, Y. Liu, J.-H. Zhang, Y. Zhao, Large-momentum effective theory, Rev. Mod. Phys. 93 (3) (2021) 035005. arXiv:2004.03543, doi:10.1103/RevModPhys.93.035005.

[5] M. Constantinou, et al., Parton distributions and lattice-QCD calculations: Toward 3D structure, Prog. Part. Nucl. Phys. 121 (2021) 103908. arXiv:2006.08636, doi:10.1016/j.ppnp.2021.103908.

[6] H.-W. Lin, Overview of Lattice Results for Hadron Structure, Few Body Syst. 64 (3) (2023) 58. doi:10.1007/s00601-023-01842-9.

[7] X. Ji, Parton Physics on a Euclidean Lattice, Phys. Rev. Lett. 110 (2013) 262002. arXiv:1305.1539, doi:10.1103/PhysRevLett.110.262002.

[8] J. Holligan, H.-W. Lin, Systematic improvement of x-dependent unpolarized nucleon generalized parton distributions in lattice-QCD calculation, Phys. Rev. D 110 (3) (2024) 034503. arXiv:2312.10829, doi:10.1103/PhysRevD.110.034503.

[9] R. Zhang, J. Holligan, X. Ji, Y. Su, Leading power accuracy in lattice calculations of parton distributions, Phys. Lett. B 844 (2023) 138081. arXiv:2305.05212, doi:10.1016/j.physletb.2023.138081.

[10] X. Gao, A. D. Hanlon, S. Mukherjee, P. Petreczky, Q. Shi, S. Syritsyn, Y. Zhao, Transversity PDFs of the proton from lattice QCD with physical quark masses, Phys. Rev. D 109 (5) (2024) 054506. arXiv:2310.19047, doi:10.1103/PhysRevD.109.054506.

[11] H.-W. Lin, J.-W. Chen, R. Zhang, Lattice Nucleon Isovector Unpolarized Parton Distribution in the Physical-Continuum Limit (11 2020). arXiv:2011.14971.

[12] F. Yao, et al., Nucleon Transversity Distribution in the Continuum and Physical Mass Limit from Lattice QCD, Phys. Rev. Lett. 131 (26) (2023) 261901. arXiv:2208.08008, doi:10.1103/PhysRevLett.131.261901.

[13] Z. Fan, W. Good, H.-W. Lin, Gluon parton distribution of the nucleon from (2+1+1)-flavor lattice QCD in the physical-continuum limit, Phys. Rev. D 108 (1) (2023) 014508. arXiv:2210.09985, doi:10.1103/PhysRevD.108.014508.

[14] R. Zhang, H.-W. Lin, B. Yoon, Probing nucleon strange and charm distributions with lattice QCD, Phys. Rev. D 104 (9) (2021) 094511. arXiv:2005.01124, doi:10.1103/PhysRevD.104.094511.

[15] S. Bhattacharya, K. Cichy, M. Constantinou, J. Dodson, X. Gao, A. Metz, S. Mukherjee, A. Scapellato, F. Steffens, Y. Zhao, Generalized parton distributions from lattice QCD with asymmetric momentum transfer: Unpolarized quarks, Phys. Rev. D 106 (11) (2022) 114512. arXiv:2209.05373, doi:10.1103/PhysRevD.106.114512.

[16] S. Bhattacharya, et al., Generalized parton distributions from lattice QCD with asymmetric momentum transfer: Axial-vector case, Phys. Rev. D 109 (3) (2024) 034508. arXiv:2310.13114, doi:10.1103/PhysRevD.109.034508.

[17] H.-W. Lin, Nucleon Tomography and Generalized Parton Distribution at Physical Pion Mass from Lattice QCD, Phys. Rev. Lett. 127 (18) (2021) 182001. arXiv:2008.12474, doi:10.1103/PhysRevLett.127.182001.

[18] H.-W. Lin, Nucleon helicity generalized parton distribution at physical pion mass from lattice QCD, Phys. Lett. B 824 (2022) 136821. arXiv:2112.07519, doi:10.1016/j.physletb.2021.136821.

[19] K. Cichy, et al., Generalized Parton Distributions from Lattice QCD, Acta Phys. Polon. Supp. 16 (7) (2023) 7–A6. arXiv:2304.14970, doi:10.5506/APhysPolBSupp.16.7-A6.

[20] A. Avkhadiev, P. E. Shanahan, M. L. Wagman, Y. Zhao, Determination of the Collins-Soper Kernel from Lattice QCD, Phys. Rev. Lett. 132 (23) (2024) 231901. arXiv:2402.06725, doi:10.1103/PhysRevLett.132.231901.

[21] M. A. Ebert, S. T. Schindler, I. W. Stewart, Y. Zhao, Factorization connecting continuum & lattice TMDs, JHEP 04 (2022) 178. arXiv:2201.08401, doi:10.1007/JHEP04(2022)178.

[22] T.-J. Hou, H.-W. Lin, M. Yan, C. P. Yuan, Impact of lattice $s(x) - \bar{s}(x)$ data in the CTEQ-TEA global analysis, in: Snowmass 2021, 2022. arXiv:2204.07944.

[23] A. Ablat, S. Dulat, T.-J. Hou, H.-W. Lin, K. Xie, C. P. Yuan, Impact of lattice gluon dataset on CTEQ-TEA global PDFs (2 2025). arXiv:2502.10630.